JOURNAL OF MATERIALS SCIENCE 11 (1976) 57–70

The fracture toughness of conventional materials and composite systems containing non-fracturing reinforcing elements

M. J. CHAPPELL, J. G. MORLEY
Wolfson Institute of Interfacial Technology, University of Nottingham, UK

A preliminary study has been made of the fracture surface energies and modes of failure of unidirectionally reinforced fibrous composites containing bicomponent (duplex) reinforcing elements with non-fracturing cores. Local high stress concentrations have been produced by the use of severely notched specimens of the Tattersall and Tappin type which have been tested in three-point bending. Comparisons have been made with conventional materials tested under similar conditions. It has been shown that the duplex fibre-reinforced specimens are able to support a substantially constant load up to deformations at which conventional materials have either failed completely or are able to support only relatively negligible bending loads. The effective fracture surface energies of experimental duplex fibre systems subjected to this degree of deformation are of the same order of magnitude, on a weight for weight basis, as those of the toughest available metal alloys. It is observed that when the permanently deformed duplex fibre systems are subjected to further deformations of a cyclic nature within the relevant elastic range of the material, relatively large amounts of energy are absorbed by frictional losses during decoupling and recoupling of the core–sheath interface. Possible reasons for this are discussed. The influence of transverse reinforcement on the generation and development of secondary matrix cracks has also been investigated.

1. Introduction

Fracture toughness is an important property of any fibre composite. It can be assessed in terms of the fracture surface energy of the material (γ_f), which may be defined empirically as the minimum amount of energy required to create unit area of fracture surface. As such it gives an indication of the ability of the material to resist crack propagation. When fibrous composites or other coventional structural materials are subjected to local high stress concentrations the resulting failure process is localized. This is so whether the material in question is brittle or ductile. A convenient mechanical test which enables a high local stress concentration to be applied to both brittle and ductile materials has been devised by Tattersall and Tappin [1]. This test has been used in the present work to provide a standard of comparison between the effective fracture surface energies of (a) orthodox materials (including unidirectionally reinforced fibre composites) and (b) fibrous composites in which the primary reinforcing phase is arranged not to fracture.

Fibre fracture may be prevented by a stress controlled decoupling of the interface between the primary reinforcing element and the rest of the composite structure. This type of mechanism has been discussed in detail by Morley [2] and Morley and Millman [3]. The application of this principle in linear energy absorbing devices has been described [4], and the ability of duplex reinforcing fibres to arrest matrix crack growth under certain circumstances in composite materials has also been reported [5]. This paper is

concerned with an investigation of the potential contribution of non-fracturing reinforcing elements to energy absorption within a fibrous composite structure.

Bicomponent, core–sheath (duplex) reinforcing elements in which the core has non-fracturing characteristics have been produced and encapsulated in an epoxy resin matrix to form the basic composite structures employed in this work. These experimental duplex reinforcing elements were fabricated using various combinations of high strength piano wire or stainless steel wire as the core element and stainless steel hypodermic tube as the sheath. The core wire was formed into an elongated helix of external diameter when unstressed somewhat greater than the internal diameter of the tube by a method described elsewhere [3, 6]. This ensures that when the wire is drawn into the tube there is a pressure exerted along the line of contact and hence a frictional force resisting further displacement of the wire within the tube. As the tensile load carried by the helical core wire is increased, it undergoes a lateral contraction so that the pressure which it exerts on the wall of the tube is dimished and the shear strength of the frictional interface is correspondingly reduced.

A simple analysis of the situation [6] indicates that complete debonding should occur when the diameter of the helix is reduced to that of the internal diameter of the tube. Neglecting torsion and shear effects, the load L_{max}, required to cause core–sheath debonding and subsequent pull-through of the core is given by,

$$L_{max} = \frac{EI}{r_2 \sin \alpha_2}\left[\frac{\cos^2\alpha_1}{r_1} - \frac{\cos^2\alpha_2}{r_2}\right] \quad (1)$$

where r_1 and r_2 are the distances between the axis of the helix and the centre of the wire when respectively outside and inside the tube, and α_1 and α_2 are the corresponding helix angles. E and I are respectively the Young's modulus and cross-sectional geometrical moment of inertia of the core wire.

The frictional shear strength (τ_σ) of the core–sheath interface at a particular core stress σ has been observed to change linearly with the stress carried by the core wire both in tension and compression [3] so that,

$$\tau_\sigma = \tau_0(1 - \sigma/\sigma_{max}) \quad (2)$$

where τ_0 is the shear strength of the core–sheath interface when the local core wire stress is zero and σ_{max} is the maximum pull-through stress (i.e. L_{max}/A, where A is the cross-sectional area of the core wire). It follows that, provided $\sigma_{max} < \sigma_{ult}$ (the tensile breaking stress of the core wire), fracture of the core wire cannot occur. The stress distribution along a cylindrical core wire of radius r, as it is either pulled out of or pushed into the tube is given by,

$$\sigma_x = \sigma_{max}\{1 - \exp(-2\tau_0 x/\sigma_{max} r)\} \quad (3)$$

where x is the distance measured from the free end of the wire (Fig. 1). The shear strength of the

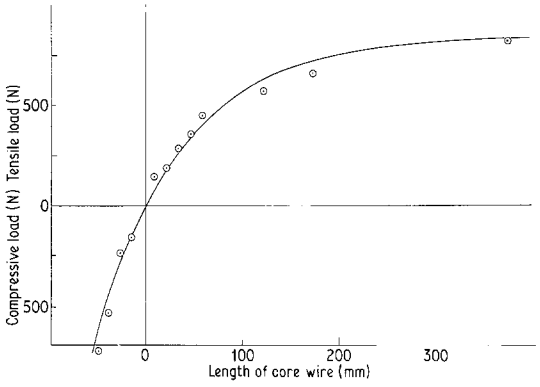

Figure 1 Compressive (C) and tensile (T) loads required to cause the longitudinal displacement of various lengths (x) of core elements (taken from [3]).

fibre–matrix interface at the corresponding position is given by [5],

$$\tau_x = \tau_0 \exp(-2\tau_0 x/\sigma_{max} r). \quad (4)$$

Methods of determining the value of the shear strength of the core–sheath interface under various conditions are discussed in detail elsewhere [7].

When these bicomponent elements are employed as reinforcing fibres within a composite structure, the core and sheath are effectively locked together and behave as a homogeneous reinforcing fibre until the interfacial frictional forces are reduced sufficiently to allow differential movement to occur. When the sheath element fails in tension the load carried locally by the bicomponent reinforcing element is reduced by an amount equal to the contribution of the sheath prior to failure. However, if failure of the sheath element occurs while the stress carried by the core is less than σ_{max}, the crack bridging core fibre can carry an increasing tensile stress with increasing composite deformation up to the limiting value

of σ_{max}. The local shear strength of the fibre–matrix interface falls as the local fibre tensile stress rises and the effective length of bridging fibre undergoing elastic extension, therefore, increases until the stress distribution is synonymous with that described by Equation 3. Further extensions of the composite structure cause the core fibre to be pulled bodily through the sheath against frictional forces, thereby absorbing considerable amounts of energy and increasing the fracture toughness of the composite structure.

2. Experimental

2.1. Specimen fabrication

Duplex fibre-reinforced composite specimens for fracture surface energy determinations were fabricated by encapsulating the bicomponent elements in an epoxy resin matrix. The stainless steel hypodermic tubes were conveniently distributed within the matrix by using a jig arrangement consisting of aligned squares of aluminium micromesh gauze suitably positioned in the mould prior to casting (Fig. 2). Whilst this procedure facilitated specimen fabrication it had the relative disadvantage of resulting in a fairly low volume fraction of fibre reinforcement (~ 10%). Although the gauze mesh size varied slightly from sample to sample, care was taken to utilize identical gauze throughout each series of experiments in order to maintain a constant tube distribution within the matrix. In view of the reported effects of resin curing conditions on fibre matrix interfacial bond strengths [8], close control was maintained over casting conditions during the present work. Specimens were cast in a mould preheated to 135° C using Araldite CT200 with HT901 hardener (100: 30) and cured overnight at this temperature before being allowed to cool gradually to room temperature.

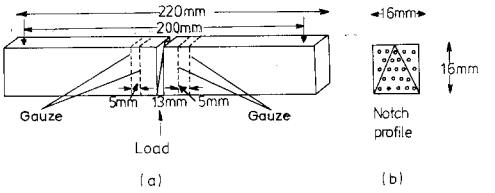

Figure 3 Configuration of specimens for fracture energy determinations (a) specimen dimensions and loading arrangement (b) notch profile.

Specimens with approxmate overall dimensions 16 mm x 16 mm x 220 mm (Fig. 3a) were produced in this manner. Helically wound wire core fibres with a suitable length of straight tail were prepared as described elsewhere [6]. Assembly of the bicomponent elements was carried out by consecutively threading the straight portion of each core fibre into the appropriate tube and then loading the wire in tension so that the elastic lateral contraction of the helix was just sufficient to allow the tube to be slid into position. In this manner core wires were inserted into the fifteen tubes contained within the triangular cross-sectional area indicated in Fig. 3b. This ensured that the isosceles triangular cross-section which remained after the specimen had been notched, as described later, was reinforced by an evenly distributed array of duplex elements. Three 220 mm lengths of resin encapsulated tubing were normally mounted in close contact on each wire in order to ensure that sufficient core–sheath stress transfer length was available for generation of the maximum core fibre pull-out stress during subsequent testing. After each core wire was inserted, the tensile load, which was approximately equivalent to the pull-through load, was removed, thus allowing the core fibre to expand laterally and thereby exert a contact pressure on the wall of the tube. The properties of the various wire–tube combi-

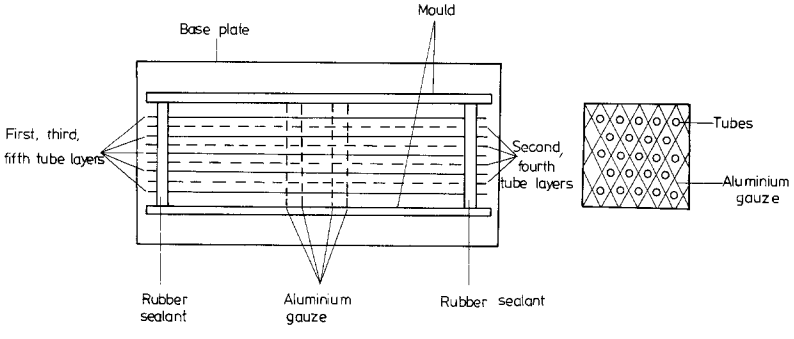

Figure 2 Arrangement of tube elements within the mould during casting.

TABLE I Properties of duplex reinforcing fibres

System reference	Wire type	Music wire gauge no. (m.w.g.)	Wire diameter (mm)	Initial helix external amplitude (mm)	Initial helix wavelength (mm)	Stainless steel tube gauge no.	Tube internal diameter (mm)	Pull-through load (N)
(a)	Piano	10	0.61	0.85	6.0	19*	0.77	330 – 350
(b)	Stainless steel	–	0.61	0.88	6.0	19*	0.83	250
(c)†	Piano	11	0.66	0.87	6.4	19*	0.83	400 – 430
(d)‡	Piano	12	0.73	1.00	~ 6.5	19*	0.82	~ 600

† Some minor plastic deformation occurring during core–sheath pull-through.
‡ Elastic-plastic system – asymmetric pull-in/pull-out (see Section 3.1).
* Indicates special thin wall tube.

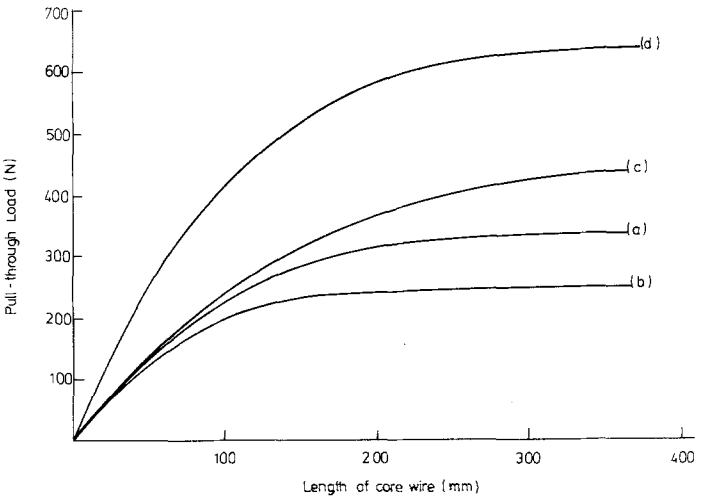

Figure 4 Typical experimental pull-through curves for the duplex systems employed in this work (Table I).

nations employed in this work are summarized in Table I. Typical experimental core load distributions corresponding to an expression analogous to Equation 3 above are illustrated in Fig. 4.

2.2. Experimental procedure

All three-point bend specimens were notched centrally in the manner of Tattersall and Tappin [1] by means of a 1.05 mm thick diamond slitting wheel, thereby reducing the square cross-section to an isosceles triangular section (Fig. 3b). The geometry of this notch arrangement normally ensured that when the specimen was loaded in three-point bending as illustrated in Fig. 3a, a high enough stress concentration existed at the apex of the triangular section to initiate crack growth in this region before sufficient elastic energy became available to cause catastrophic failure to occur even in the case of a fairly brittle material. The deflecting load was applied by means of a standard three-point bend rig mounted on the cross-head of an Instron tensile test machine. This rig enabled specimens to be loaded over a span of 50, 100, 150 or 200 mm.

Fracture surface energy determinations were normally carried out at a low rate of deflection using a "hard" 5000 N load cell (approximate deflection 9×10^{-4} cm N^{-1} load) which was only able to absorb small amounts of elastic energy. This arrangement ensured that crack propagation normally took place in a controlled manner so that the failure was contained within the specimen and no work was expended in the form of kinetic energy, as would have been the case if the two halves were thrown apart following complete rupture of the specimen. Thus, providing fracture proceeds in the type of non-catastrophic manner illustrated, for example, in Fig. 5c, all the elastic energy initially stored in the system is, in principle, converted into fracture energy as the applied load falls to zero.

2.3. Determination of fracture surface energies

Since complete failure of the duplex composites could not be induced by means of this type of three-point bend test, these specimens were normally loaded over a span length of 200 mm until a fixed vertical machine cross-head displacement of 20 mm had been obtained; complete failure of the orthodox materials tested normally occurred well before this limit had been reached. A cross-head speed of 0.05 cm min^{-1} was normally employed in these experiments. Typical load extension curves adjusted for relative density considerations by factoring for the appropriate specific gravity are shown schematically in Fig. 5 which includes examples of a duplex composite, a "conventional" composite and various orthodox materials. In this context the term "conventional" composite is taken to imply one in which the reinforcing fibres take the form of empty stainless

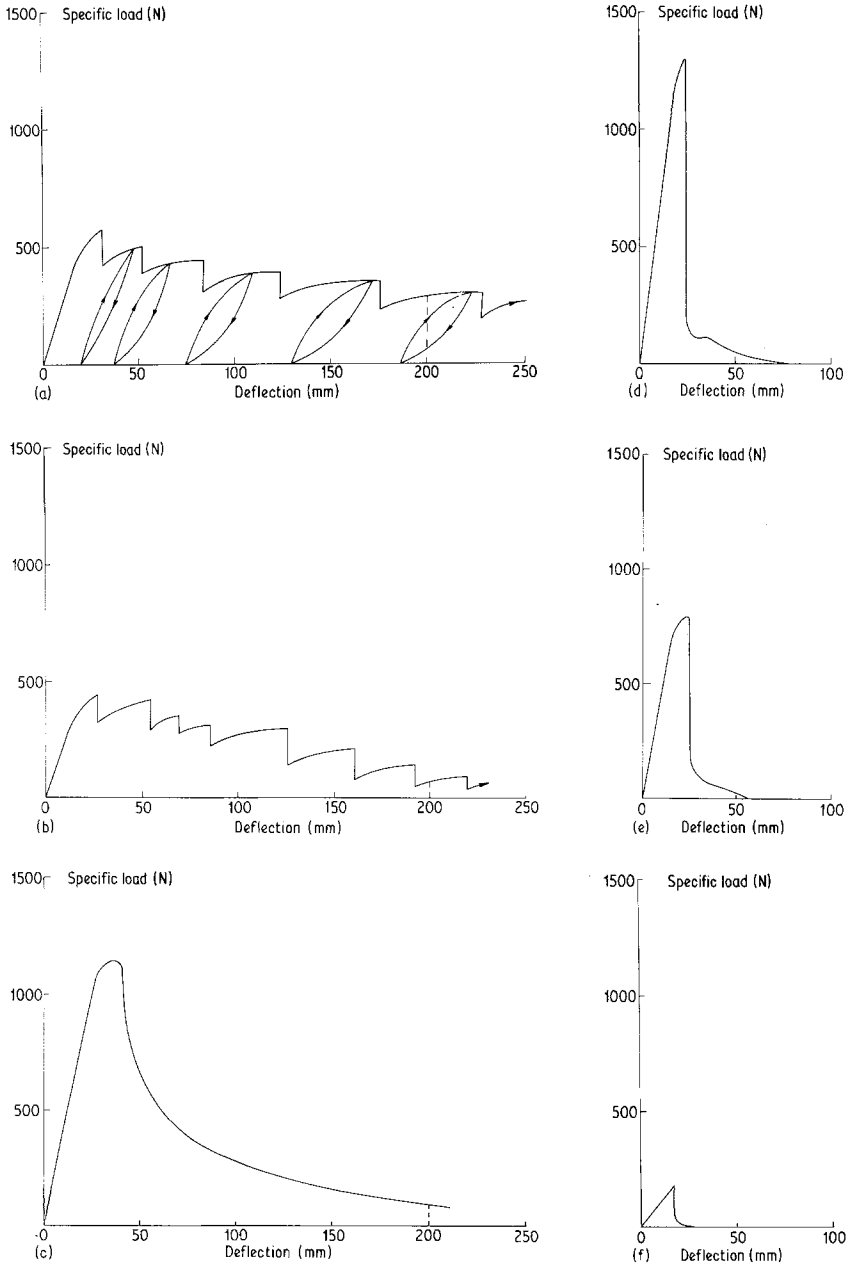

Figure 5 Typical load–deflection curves from fracture energy determinations. (a) Duplex composite, (b) conventional composite, (c) aluminium, (d) duralumin, (e) mild steel, (f) polymethyl methacrylate.

TABLE II Comparative fracture surface energies for a range of materials

Material	Average fracture surface energy* γ_f (J m^{-2} × 10^{-4})	Specific gravity	Specific fracture surface energy* (J m^{-2} × 10^{-4})
Aluminium	8.6	2.7	3.2
Typical duplex composite (system a)	5.0	1.7	2.9
Mild steel	4.8	7.8	0.6†
"Conventional" composite	2.7	1.5	1.8
Hardened‡ duralumin	2.1	2.8	0.8†
Teak wood	0.8 – 1.6§	0.8	1.0 – 2.0†
Epoxy resin (CT200/HT901)	0.1	1.2	0.1¶
Polymethyl-methacrylate	0.1	1.2	0.1¶

* Measured to a fixed cross-head deflection of 20 mm.
† Complete failure of specimen occurred at a deflection less than 20 mm.
‡ Aircraft alloy supplied by R.A.E., Farnborough.
§ Dependent on grain direction.
¶ Brittle failure.
"Conventional" composite refers to stainless steel hypodermic tubes cast in resin.

TABLE III Comparative fracture surface energies for duplex fibre-reinforced materials and conventional composites*

Sample type	Reinforcement spacing (m × 10^{-3})	Average fracture surface energy, γ_f (J m^{-2} × 10^{-4})	Maximum failing load (N)	Interlaminer shear strength (MN m^{-2})
System (a)				
Conventional composite	–	2.8	640	6.9
Duplex	–	5.1	870	–
Conventional composite	6	2.7	660	7.4
Duplex	6	5.0	880	–
Conventional composite	13	2.5	670	7.7
Duplex	13	5.1	890	–
Conventional composite	25	2.7	680	7.5
Duplex	25	5.0	840	–
System (b)				
Conventional* composite	–	2.1	590	–
Duplex	–	4.3	790	–
Conventional composite	6	2.0	630	–
Duplex	6	4.3	780	–
Conventional composite	13	2.1	580	–
Duplex	13	4.7	800	–
Conventional composite	25	1.9	570	–
Duplex	25	4.8	820	–

* "Conventional" composite refers to stainless steel hypodermic tubes cast in resin.

steel hypodermic tubes (i.e. tubes identical to those employed to produce duplex elements but without any convoluted core fibres).

The effective fracture surface energy (γ_f) of each specimen was calculated from the area under the relevant experimental load–extension curve. This was measured using a Haff 315 planimeter, an average of at least three readings being taken on each occasion. These areas were converted into the equivalent energy values and the corresponding fracture surface energies shown in Tables II and III were calculated from the expression,

$$\gamma_f = \frac{\text{Energy absorbed during specimen deformation}}{2 \times \text{cross-sectional area of specimen}} \quad (5)$$

The nominal triangular cross-sectional area of the specimen estimated from the overall dimensions was employed in this equation to calculate the effective fracture surface energy as it was often virtually impossible to measure the real area of new surface created during specimen fracture, particularly in the case of the composite materials where multiple cracking and splitting usually occurred. The average values of fracture energy for the various materials were calculated from at least three determinations in each case. Specific values were obtained for each material by dividing by the appropriate specific gravity, (i.e. relative density).

2.4. Incorporation of transverse reinforcement

Attempts were made to determine the effects of various distributions of transverse reinforcement upon the observed fracture toughness of both duplex and conventional composites. The aluminium gauze formers employed to align the tubes when casting specimens provided a convenient form of cross-bracing. These gauzes were arranged in pairs 5 mm apart on either side of the Tattersall and Tappin notch (Fig. 3a). The distance between the notch and the nearest gauze of each pair in the different specimens was arranged to be approximately 6, 13 and 25 mm respectively. The average values of fracture surface energy for a series of both duplex and conventional composites with this type of transverse strengthening were determined as described above. The results are contained in Table III which for the sake of comparison also shows the equivalent values for similar composites in which no transverse reinforcement was present.

2.5. Load cycling experiments on duplex fibre-reinforced composites

Load cycling experiments were carried out in order to investigate the elastic properties of duplex systems at various stages during progressive, irreversible deformation of the specimens. Tattersall and Tappin type specimens similar to those already described were again employed. Normally, the bending load applied to the specimen up to the initial failure point was increased in increments of 200 N and load cycling was carried out at each point. Following initial failure, the applied load was cycled several times along the "plateau" pull-out region which followed each successive failure, as shown schematically in Fig. 5a.

3. Results and discussion

3.1. Comparative fracture surface energies

It is obvious from Table II that the fracture energy of the duplex composite compares favourably with the best values obtained in this work for a reasonable range of conventional materials, especially on a specific basis, under the test conditions employed. The values obtained here for the fracture energies of the more orthodox materials are generally in reasonable agreement with those determined by other authors using a similar test method, but normally with specimens of much smaller dimensions [9]. In contrast to the observations of Tattersall and Tappin [1] on smaller specimens, a reasonably clean fracture with a crystalline appearance of the fracture face (analogous to that produced with mild steel) was obtained in the case of the aluminium specimens which exhibited a relatively large value of fracture energy. The hardened duralumin specimens, however, gave much lower values than those determined in the earlier work ($1.4 \times 10^5 \text{ J m}^{-2}$) [1]. This is perhaps to be anticipated in view of the comparatively high UTS ($\sim 500 \text{ MN m}^{-2}$) of this particular material. The fracture energy of a duralumin specimen of slightly different composition and somewhat lower UTS ($\sim 350 \text{ MN m}^{-2}$) was intermediate between that of the hardened material and the commercially pure aluminium.

The fracture energies of the teak wood specimen varied considerably with the grain orientation. Fracture normal to the wood grain was associated with a large amount of fibrous pull-out and hence

the higher values of fracture energy. Fracture in a direction approximately parallel to the grain resulted in a predominance of interlaminar splitting and a comparatively reduced fracture energy. The polymethyl methacrylate (perspex) and epoxy resin specimens exhibited "mirror" type fracture faces. Failure occurred in a predominantly brittle fashion under the conditions employed and these specimens did not strictly fulfil the requirements of the Tattersall and Tappin [1]. Little significance can, therefore, be attached to the absolute values of fracture surface energy obtained for these particular materials in this investigation. A few tests carried out on the various materials using a specimen span length of 150 mm usually resulted in a relative increase in the experimentally observed failure load; this was almost invariably accompanied by a corresponding reduction in the fracture surface energy measured to the standard fixed deflection.

The Tattersall and Tappin test has also been widely employed to determine the effective fracture surface energies of more orthodox types of composite material. For instance, values ranging from 0.3 to $6 \times 10^4 \, J \, m^{-2}$ have been obtained for various types of CFRP [10–12]. Similarly, the incorporation of carbon fibres within various types of ceramic material (e.g. pyrex glass) has been found to increase the fracture energy by roughly three orders of magnitude from a few $J \, m^{-2}$ to approximately $3 \times 10^3 \, J \, m^{-2}$ [13]. Very high fracture surface energies ($\sim 1.3 \times 10^5 \, J \, m^{-2}$) have been quoted for orthodox composites such as S-glass-reinforced epoxy resin [14] and conventional materials such as duralumin [1]. The ultimate value (i.e. at large specimen deflections) obtained for the particular experimental duplex system shown in Table II approaches that of these materials when the relative densities are taken into account.

The decrease in fracture energy on passing from duplex system (a) to system (b) (Table III) may be associated with the improved physical properties of the piano wire utilized for system (a) compared to those of the stainless steel core wire of system (b). Apart from the effects of the smaller internal diameter of the sheath used for system (a), the increased strength and modulus of the piano wire contribute significantly to the improvement in pull-through load which may be achieved for this system. Furthermore, these same properties also serve to increase the contribution of the core to the tensile strength and stiffness of these particular duplex elements prior to sheath rupture, thereby improving considerably their initial failing load. On a specific basis the highest initial failing load ($\sim 1.3 \times 10^3$ N for the hardened duralumin) observed for any material during the present work is approximately twice that of the best value obtained for a duplex composite (system c) in the three-point slow bend tests. Similarly, the specific UTS of this particular hardened duralumin has been determined as approximately $180 \, MN \, m^{-2}$ whereas that of the type of duplex composite used in the Tattersall and Tappin tests (i.e. approximately 10% volume fraction of bicomponent elements) may be calculated typically as approximately $100 \, MN \, m^{-2}$ in the direction of the fibre alignment, if it is assumed that the core element is carrying the maximum debonding load at the point of composite failure.

The UTS of the duplex composites may be improved significantly by increasing the volume fraction of reinforcing elements in the specimen. Thus, at approximately 70% volume fraction of reinforcing elements the UTS of a typical duplex composite may be estimated as about $770 \, MN \, m^{-2}$ compared to that of $500 \, MN \, m^{-2}$ determined for the hardened duralumin. Even when the increased density of the 70% volume fraction duplex composite is taken into account, the specific UTS is still comparable to that of the hardened duralumin and considerably greater than that of a high fracture energy aluminium. An increase in volume fraction of duplex elements is also potentially advantageous in that it should produce a corresponding increase in fracture energy. It should be feasible to improve the specific UTS values of duplex materials by utilizing core fibres consisting of lightweight resin-bonded carbon fibres in place of the convoluted steel wires. Still further improvements might be made by fabricating the complete duplex element from strong, stiff lightweight ceramic materials. Preliminary experiments to produce this latter type of bicomponent reinforcing fibre have been described elsewhere [15]. Alternatively, the addition of further strategic reinforcement to the type of resin matrix duplex system described here (e.g. in the form of high strength wires or carbon fibres), or even the encapsulation of the duplex elements in a metal matrix should enable the failing stress to be significantly increased whilst maintaining a potentially high energy absorbing capacity.

Some improvements in the duplex composite

fracture energy have been demonstrated using system (c) (Table I). This latter system, which involves some plastic deformation of the core wire, gives rise to a fracture surface energy in excess of $6 \times 10^4 \, J \, m^{-2}$ and further increases should be attainable using different geometrical core–tube arrangements. The effective fracture energy of system (d) which involves a large initial pull-through load and a substantial amount of plastic deformation of the core wire is only intermediate between the values for systems (a) and (b). This experimental value may be compared with the calculated fracture energy which is apparently substantially larger than the values obtained for the other duplex systems. It seems probable that sufficient over-load was applied to the wires during specimen assembly to reduce significantly the pull-through load compared to the value quoted in Table I for this particular system, which undergoes considerable plastic deformation during pull-through. This unsymmetrical pull-in/pull-out situation has been discussed for the case of other systems involving plastic core deformation [3, 16]. If these non-elastic core duplex elements were constructed, for instance, by drawing down the tube onto the core, this unfavourable situation during initial deformation could be avoided, thereby enabling the plastic component of core deformation to make a full contribution to the fracture energy.

It should also be pointed out that the particular specimen notch configuration employed in these tests is disadvantageous in the case of the duplex composites. A very large proportion of the initial load must be supported in the first instance by the single duplex element at the apex of the triangular cross-section and the major contribution to the fracture energy will be made by elements in this region. It would not seem unreasonable, therefore, to anticipate a significant improvement in relative fracture surface energy if an orthodox planar sawcut notch was employed. A much higher concentration of duplex elements than the somewhat low volume fraction of approximately 10% that was employed in this work for the sake of convenience of specimen assembly would also significantly increase the fracture energy as mentioned previously.

Furthermore, it should be emphasized that the duplex specimens had only partially failed even at the relatively large deformations to which they were subjected during these slow bend tests (Fig. 5a) and remained, to some considerable degree, relatively elastic in their response to load cycling treatment (Section 3.4). In comparison, almost all orthodox materials and a large proportion of fibre reinforced composites would effectively have failed completely at such deflections (e.g. Fig. 5b to f). Even the aluminium which exhibited a slightly larger overall fracture surface energy than the duplex composite under these test conditions was absorbing energy at only half the rate of the duplex material at a cross-head displacement of 20 mm (Fig. 5a and c).

Further increases in specimen deflection result in even greater differences in the rate of energy absorption since the load bearing capacity of the aluminium continues to fall fairly rapidly in comparison to that of the duplex material which maintains a relatively high energy absorbing capacity even at large deflections. This high energy absorbing capacity results from the ability of the duplex composites to diffuse the initial, highly localized energy absorption from the immediate vicinity of the notch and redistribute this energy in a more easily assimilated form throughout the composite structure.

3.2. Calculated values of fracture surface energy

Attempts were made to estimate the approximate fracture energies of the various duplex composites from the measured geometrical parameters of each system. The angle of specimen deflection from the horizontal was determined for each system at the conclusion of the experiment (i.e. at a fixed vertical machine cross-head displacement of 20 mm) and this was equivalent to half the angle of crack opening at the notch. Assuming that the specimens pivoted about a point in the plane of the bottom layer of tubes, it was then possible to calculate the amount of wire pulled out of each layer of tubes from a knowledge of the tube spacing, which was governed by the particular mesh size of the gauze employed. The approximate amount of energy absorbed in wire pull-through was then determined from the product of the summation of these wire pull-out lengths over the total number of elements within the notch area and the known core pull-through load. The addition of an amount of energy equivalent to that required to rupture the corresponding tube–matrix conventional composite to these pull-through energies then enabled an estimate of the overall duplex fracture energy to be

TABLE IV Calculated and experimental fracture surface energies of duplex composites at a cross-head deflection of 20 mm.

System reference	Calculated* pull-through energy ($J m^{-2} \times 10^{-4}$)	Maximum fracture surface energy of tubes in resin* ($J m^{-2} \times 10^{-4}$)	Total calculated fracture surface energy ($J m^{-2} \times 10^{-4}$)	Experimental fracture surface energy γ_f ($J m^{-2} \times 10^{-4}$)
(a)	3.3	2.7	6.0	5.1
(b)	2.8	2.0	4.8	4.3
(c)	5.8	2.0	6.8	6.2
(d)	5.9	2.0	7.8	4.8

* Based on experimental values for equivalent "conventional" composites.

made for the conditions employed in these experiments.

In view of the approximations involved in this calculation, these values (Table IV) are in reasonable agreement with those determined experimentally for the various duplex systems. The tendency of the calculation to apparently somewhat over-estimate the fracture energies is attributable to several factors; these are principally (a) the difficulty of locating the exact bending fulcrum of each specimen and (b) the probability that smaller amounts of energy are actually expended in propagating matrix cracks in the duplex systems than in the equivalent conventional tube composites (Section 3.3). These considerations must be offset, however, by the fact that no account has been taken of the frictional work of debonding involved in the decoupling process (though this should be negligible in comparison with the energy dissipated in frictional losses as the cores are pulled through the tubes) and the increase in apparent pull-through load caused by the non-axial alignment of the pull-out load, which becomes more significant with increasing deflection.

3.3. Effects of transverse reinforcement

The presence of the transverse reinforcement did not significantly alter the fracture surface energies of the conventional composites (Table III) where any effects due to variations in the distribution of gauze might be expected to be most readily apparent. The gauze appeared to reduce the tendency for major interlaminar cracks to occur. Normally, these cracks propagated principally along the fibre–matrix interface of the bottom layer of tubes and split the specimen longitudinally for some distance. However, when the gauze was present, a larger number of small cracks were initiated in the area of the failure and these showed a greater tendency to eventually deflect at right angles to the fibres in the region of the gauze. The overall effect of the transverse reinforcement, therefore, seemed to be to alter the pattern of matrix cracking rather than to change the absolute amount of energy absorbed in this manner. The complexity of the matrix cracking precluded any further conclusions being drawn in this direction.

The manner in which many of the multiple matrix cracks which occurred during fracture were eventually deflected away from the interlaminar planes and into the bulk matrix in a direction normal to the fibre reinforcement, indicated that relatively strong bonding had occurred at the tube–matrix interface. This was confirmed by comparative measurements of the transverse tensile strength of specially prepared resin specimens containing either a single layer of transversely distributed hypodermic tubes or a similar single layer of tubes reinforced at 90° by two parallel strips of aluminium gauze (i.e. aligned in the loading direction). The results of these tests showed that very little change occurred in transverse tensile strength in the presence of tubes and gauze compared to that determined for the resin matrix alone. The relatively strong fibre matrix bond might be expected to minimize interlaminar shear failure and reduce the effect of the transverse reinforcement.

Values of interlaminar shear strength were determined for one series of gauze-reinforced composites (system a) by means of conventional short beam interlaminar shear tests. The bend rig employed for the fracture energy determinations was again used, but on this occasion with a specimen span to depth ratio of approximately six. The experimental values of interlaminar shear strength, which are included in Table III, are reasonably constant, and this confirms, therefore, that the transverse reinforcement has no significant effect on the composite longitudinal shear properties. Little significance can be attached to the absolute

values of interlaminar shear strength since the method of measurement tends to be inaccurate for composites containing low volume fractions of reinforcing fibres tested at aspect ratios similar to that employed here. In view of the relatively strong fibre–matrix interfacial bond strength, these results essentially provide an indication of the shear strength of the matrix.

The fracture energies of the duplex composites again show little effect of gauze distribution other than that attributable to normal experimental error. This might be anticipated since the energy absorbed by matrix cracking and delamination in duplex composites which would indicate that cases compared with that of frictional debonding and pull-through. There appeared to be some reduction in the amount of matrix cracking in the duplex composites which seemed to indicate that the amount of energy absorbed by this means was reduced in comparison to the equivalent conventional composites. The somewhat greater variability of the fracture energies of the second series of duplex composites (system b) is most probably attributable to the unsatisfactory nature of some of the notches machined into these specimens. A careful analysis of crack growth conditions might reveal more significant aspects of the relative behaviour of the duplex systems and conventional composites under the influence of different distributions of transverse reinforcement.

3.4. Load deflection curves and energy losses during elastic cycling of duplex fibre composites

As prepared the core elements are initially in residual tension at the position of the notch, with the rest of the composite structure in residual compression. Prior to the onset of composite failure, the load cycling behaviour of each specimen is reproducible and sensibly elastic apart from some slight hysteresis losses which are probably attributable to a combination of frictional effects occurring during initial decoupling of the prestressed core wires and machine error. As the specimen is deformed further following initial failure, progressive fracture of the tube elements occurs and the core elements are drawn through the tubes. The stress level at the crack face is given by Equation 3. If the load applied to the specimen is then reduced to zero the specimen becomes straighter under the influence of the elastic deflections of the portions of the material which remain intact. When the specimen is of appreciable length, the core elements cannot be pushed back through the tubes because the compressive forces required to do this are too large as a result of the exponential form of Equation 3 (see also Fig. 1). The specimen therefore takes up an equilibrium position with a stress distribution along the core element similar to that indicated in Fig. 6a.

The line A A′ represents the initial position of the notch and the stress (T) represents the initial maximum tensile stress, σ_x, developed in the core wire as the specimen is being deformed. The magnitude of the compressive stress (C) is governed by the magnitude of the restoring forces developed by the as yet unfractured portion of the specimen. It is clear that in an ideal system with uniform properties the tensile section of the stress distribution curve must be symmetrical as indicated. This is so since the local rate of shear stress transfer is governed by the local tensile load carried by the core reinforcing element. The stress transfer across the core–tube interface must, therefore, conform to Equation 3, or be zero if the strain in tube and core are equal. If the magnitude of the compressive stress is substantially less than that indicated in Fig. 6a, the equilibrium stress distribution along the core in an ideal system can be supposed to take the form indicated in Fig. 6b.

As the load is reapplied to the specimen to cause its elastic deflection, the stress distribution along the core element changes sequentially as indicated by curves 1, 2, and 3 etc, in Fig. 6c and d. The relative stiffness of the crack bridging core elements is, therefore, initially large because only a relatively short length of core wire is undergoing elastic deformation. As the deflection proceeds, a progressively increasing length of core wire is being extended elastically so that the relative stiffness of the system would be expected to fall. This is confirmed qualitatively by the changes occurring in the experimentally observed cross-head deflection curves with increasing load as shown schematically in Fig. 5a.

Typical experimental curves also show a sudden increase in apparent stiffness of the specimen as the direction of the cross-head movement of the testing machine is reversed. This can be accounted for by the unstable nature of the recoupling process when compressive loads are applied (Fig. 1). This condition is likely to be aggravated in the particular arrangement employed by the non-axial loading of the core elements. As a result, the stress distribution

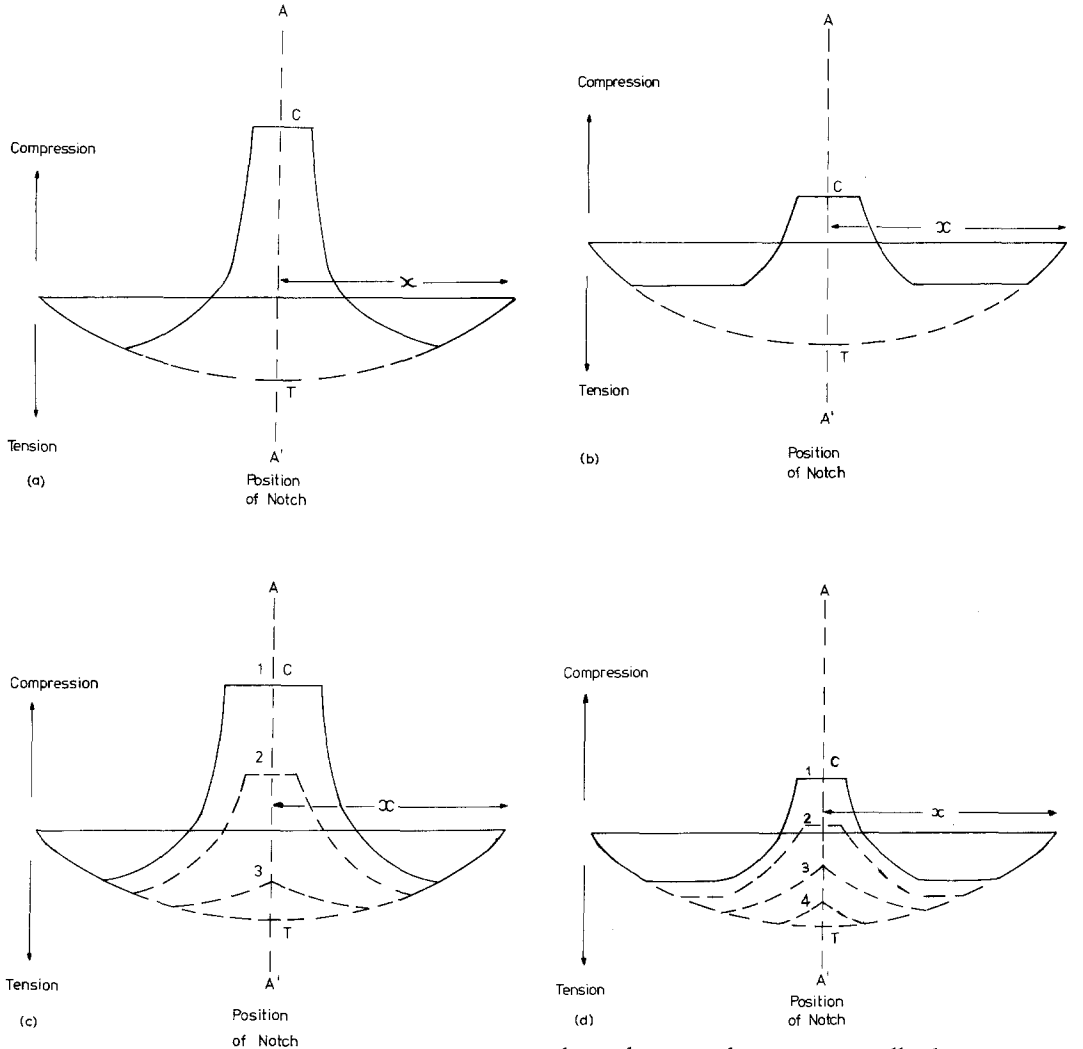

Figure 6 Idealized stress distribution along a core element during load cycling.

along the core element may well take up a sequential series of configurations as indicated by curves 1, 2 and 3 in Fig. 6e in returning to the Fig. 6c distribution, instead of following an exact reversal of the extension sequence. A stress redistribution process of this type could account qualitatively for the observed relatively constant stiffness of the specimen as the applied load is reduced. Whatever the precise nature of the stress redistribution processes occurring, it is clear from Fig. 5a that considerable amounts of energy are being absorbed, presumably by frictional losses, during elastic deflection cycling of the specimen. The relative amount of energy absorbed also increases as the extent of the deflection (and hence the number of tube elements which have fractured) increases.

4. Conclusions

The behaviour of fibrous composites containing non-fracturing reinforcing elements has been

shown to differ from that of other materials in various ways when carrying out fracture energy determinations using Tattersall and Tappin type slow bend tests. Firstly, the load bearing capacity of these core elements is not greatly reduced during the course of specimen deflection compared to orthodox materials, so that the specific load bearing ability of a duplex composite and its rate of energy absorption are relatively large and show a progressive improvement over the corresponding properties of other materials as deformation proceeds. The magnitude of the observed improvement is determined by the geometry of the notch arrangement employed and would be more marked with a simple planar crack than with the triangular-shaped fracture face used in this work because the amount of energy absorbed in pull-through depends, to a large extent, on the number of non-fracturing elements at the apex of the fracture face. Similarly, it should be possible to increase the relative energy and initial failing load by employing a somewhat higher volume fraction of duplex elements than that employed in the present studies.

Secondly, the stress controlled decoupling mechanism of the duplex system serves to dissipate energy from the immediate region of the crack and thereby enables the whole volume of the core element reinforcing phase to participate in the deformation process. Provided the limiting debonding stress of the core–sheath interface does not exceed the core fibre UTS then decoupling will occur, whatever the length of the specimen. Very large deflections are, therefore, possible in either a tensile or bending mode without complete rupture of the duplex material occurring.

Thirdly, energy is absorbed during elastic deformation of the specimens, probably as a result of the frictional losses associated with the decoupling –recoupling cycle of the core–tube interface. It would seem from Fig. 5a that the amount of energy absorbed in this way can form a significant proportion of the total strain energy contained within the material. The "damping capacity" of such materials when subjected to elastic perturbations would, therefore, be expected to be very high in comparison with other materials.

Additional energy absorption also results from the failure of the tube elements and the occurrence of multiple matrix cracking as in a conventional composite. Although this type of matrix cracking can be controlled to some extent by the incorporation of transverse reinforcement, the cross bracing used in these studies does not seem to affect significantly the overall amount of energy absorbed in this fashion by either the conventional or duplex composites. Approximate calculations of the fracture energies of the various duplex composites are in reasonable agreement with the experimental values considering the nature of the assumptions made. As might be anticipated, these calculations confirm that the proportion of the fracture energy absorbed in debonding and pull-through becomes increasingly dominant as the core fibre pull-out load is increased throughout a series of duplex composites. In view of these observations it may, therefore, be concluded that the "ultimate" energy absorbing capacity attainable using duplex fibre-reinforced materials should compare extremely favourably with the best value normally obtained for othodox fibre-reinforced composites and other structural materials.

Acknowledgements

The work described here forms part of a programme of basic study of composite materials supported by the Science Research Council. The authors are indebted to Mr A. Martin for invaluable assistance in fabricating specimens, to the Executive Committee of the Wolfson Institute for the provision of research facilities, and to Mr P. O'Byrne for electron microprobe analysis of the aluminium and duralumin specimens.

References

1. H. G. TATTERSALL and G. TAPPIN, *J. Mater. Sci.* **1** (1966) 296.
2. J. G. MORLEY, *Proc. Roy. Soc. London* **A319** (1970) 117.
3. J. G. MORLEY and R. S. MILLMAN, *J. Mater. Sci.* **9** (1974) 1171.
4. R. S. MILLMAN and M. J. CHAPPELL, "Report on the Fifth International Technical Conference on Experimental Safety Vechicles", London, England. (June 1974) (U.S. Government Printing Office, Washington D.C., 1975) p. 729.
5. J. G. MORLEY and I. R. McCOLL, *J. Phys. D. (Appl. Phys)* **8** (1975) 15.
6. M. J. CHAPPELL, J. G. MORLEY and A. MARTIN, *J. Phys. D: (Appl. Phys)* **8** (1975) 1071.
7. J. G. MORLEY and M. J. CHAPPELL, to be published.
8. G. A. COOPER, *J. Mater. Sci.* **5** (1970) 645.
9. D. C. PHILLIPS and A. S. TETELMAN, *Composites* **3** (1972) 216.
10. M. G. BADER, J. E. BAILEY and I. BELL, *J. Phys. D. (Appl. Phys)* **6** (1973) 572.

11. B. HARRIS, P.W.R. BEAUMONT and E. MONCUNILL de FERRAN, *J. Mater. Sci.* **6** (1971) 238.
12. P. W. R. BEAUMONT, Ph. D. Thesis, University of Sussex (1971).
13. D. C. PHILLIPS, *J. Mater. Sci.* 7 (1972) 1175.
14. P. W. BEAUMONT and D. C. PHILLIPS, *J. Comp. Mater.* **6** (1972) 32.
15. M. J. CHAPPELL and R. S. MILLMAN, *J. Mater. Sci.* **9** (1974) 1933.
16. R. S. MILLMAN and J. G. MORLEY, to be published.

Received 12 May and accepted 3 June 1975.